PROCEEDINGS OF SCIENCE

ONLINE ICRC 2021
THE ASTROPARTICLE PHYSICS CONFERENCE
Berlin | Germany
37th International Cosmic Ray Conference
12–23 July 2021

Cosmic ray energy spectrum and composition measurements from the GRAPES-3 experiment: Latest results

F. Varsi,[d,*] S. Ahmad,[c] M. Chakraborty,[a] A. Chandra,[c] S.R. Dugad,[a] U.D. Goswami,[l] S.K. Gupta,[a] B. Hariharan,[a] Y. Hayashi,[b] P. Jagadeesan,[a] A. Jain,[a] P. Jain,[d] S. Kawakami,[b] H. Kojima,[e] S. Mahapatra,[i] P.K. Mohanty,[a] R. Moharana,[j] Y. Muraki,[g] P.K. Nayak,[a] T. Nonaka,[h] A. Oshima,[e] B.P. Pant,[j] D. Pattanaik,[a,i] G.S. Pradhan,[k] P.S. Rakshe,[a] M. Rameez,[a] K. Ramesh,[a] L.V. Reddy,[a] R. Sahoo,[k] R. Scaria,[k] S. Shibata,[e] J. Soni,[d] K. Tanaka[f] and M. Zuberi[a] [The GRAPES-3 Collaboration]

[a] *Tata Institute of Fundamental Research, Homi Bhabha Road, Mumbai 400005, India*
[b] *Graduate School of Science, Osaka City University, Osaka 558-8585, Japan*
[c] *Aligarh Muslim University, Aligarh 202002, India*
[d] *Indian Institute of Technology Kanpur, Kanpur 208016, India*
[e] *College of Engineering, Chubu University, Kasugai, Aichi 487-8501, Japan*
[f] *Graduate School of Information Sciences, Hiroshima City University, Hiroshima 731-3194, Japan*
[g] *Institute for Space-Earth Environmental Research, Nagoya University, Nagoya 464-8601, Japan*
[h] *Institute for Cosmic Ray Research, Tokyo University, Kashiwa, Chiba 277-8582, Japan*
[i] *Utkal University, Bhubaneshwar 751004, India*
[j] *Indian Institute of Technology Jodhpur, Jodhpur 342037, India*
[k] *Indian Institute of Technology Indore, Indore 453552, India*
[l] *Dibrugarh University, Dibrugarh 786004, India*

E-mail: fahimwarsi89@gmail.com, pkm@tifr.res.in

The Gamma Ray Astronomy at PeV EnergieS phase-3 (GRAPES-3) experiment is located at Ooty in India (11.4° N, 76.7° E and 2200 m above m.s.l.). It consists of a densely packed array of 400 plastic scintillator detectors and a large area muon telescope (560 m^2). It measures cosmic rays from several TeV to over 10 PeV energies providing a substantial overlap with direct experiments while covering the knee region. Shower parameters are reconstructed by fitting the observed particle densities with the NKG lateral distribution function (LDF). For this analysis, the QGSJET-II-04 hadronic interaction model is used to generate the air shower simulation data for proton, helium, nitrogen, aluminium, and iron primaries. Precise measurements of the average nuclear composition are obtained by fitting muon multiplicity distributions (MMDs) for all simulated primaries with the MMDs measured by the muon telescope. Details of the analysis and preliminary results for the extracted composition and elemental energy spectrum for proton and helium from a few tens of TeV to a few PeV will be presented.

37th International Cosmic Ray Conference (ICRC 2021)
July 12th – 23rd, 2021
Online – Berlin, Germany

*Presenter

PoS(ICRC2021)388

1. The GRAPES-3 Experiment

The GRAPES-3 (Gamma Ray Astronomy at PeV Energies Phase-3) experiment is located at Ooty (11.4° N, 76.7° E, 2200 m a.s.l.), India. The GRAPES-3 extensive air shower (EAS) array consists of 400 plastic scintillator detectors of 1 m^2 area each [1, 2] and a large area muon telescope. A schematic of the array is shown in Figure 1. Each scintillator detector is shown as a filled square. The scintillator array covers an area of 25000 m^2. The scintillator detectors are arranged in hexagonal geometry to ensure the uniform selection of the EAS over the array with an inter-detector separation of 8 m. The 560 m^2 muon telescope consists of 3712 proportional counters (PRCs) each of length 600 cm and cross-section area of 10 cm × 10 cm. The PRCs are housed in 4 stations and each station has 4 modules. Each module has 4 orthogonal layers consisting of 58 PRCs in each layer [3]. It has an energy threshold of sec(θ) GeV for muons incident at zenith angle θ. A circular area of radius 50 m is used as the fiducial area for this analysis. The fiducial area (7850 m^2) is shown by a red dashed line. GRAPES-3 uses two-level trigger. The level-0 trigger is a simple 3-line coincidence in 100 ns time window and the level-1 trigger requires at least 10 detectors hit in 1 μs time window [1].

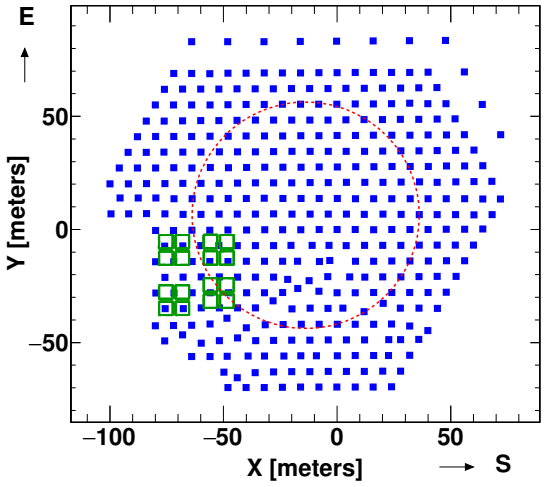

Figure 1: Schematic of GRAPES-3 EAS array. Plastic scintillator detectors (■), tracking muon telescope modules (□) and fiducial area (- - -) are shown.

Being a highly dense EAS array with an atmospheric overburden of ~800 g cm^{-2}, the GRAPES-3 experiment is capable of observing the primary cosmic rays (PCRs) from several TeV to over 10 PeV providing a substantial overlap with direct experiments. GRAPES-3 muon telescope is sensitive to PCRs composition measurements through muon multiplicity distribution.

2. Reconstruction of shower axis and shower parameters

The relative arrival time of particles and the energy deposited by the particles in each scintillator detector are recorded for every triggered shower. The shower parameters are obtained by fitting a lateral density distribution function, namely Nishimura-Kamata-Greisen (NKG) to the observed particle densities in the detectors. The NKG function is given by,

$$\rho(r, s, N_e) = \frac{N_e}{2\pi r_o^2} \frac{\Gamma(4.5 - s)}{\Gamma(s)\Gamma(4.5 - 2s)} \left(\frac{r}{r_o}\right)^{(s-2)} \left(1 + \frac{r}{r_o}\right)^{(s-4.5)}, \quad (1)$$

where N_e is the shower size, s is the shower age, r is the lateral distance from shower core (X, Y), and r_0 is the Moliere radius, for GRAPES-3, r_0 = 103 m. Reconstruction of the shower direction is a two-step process. In the first step, the relative arrival time of the EAS measured by different detectors is used to reconstruct its arrival direction by fitting it with a plane front. In the second

step, a more accurate shower arrival direction is obtained by correcting it with shower size and shower age [4].

3. Quality selection cuts and experimental data

To ensure the quality of the data used for analysis, the following event selection criteria are used.

- Events with successful shower parameter reconstruction are used.
- Events with successful shower arrival direction reconstruction are used.
- The reconstructed cores must lie within the fiducial area. In this way, most of the improperly reconstructed EAS, due to EAS core landing near the edge or outside the array can be avoided.
- The reconstructed age parameter is restricted to lie between 0.2 and 1.8.
- Zenith angle is restricted to be less than 18°.
- Shower size (N_e) > 10^4 corresponding to trigger efficiency greater than 90% are used.

Data collected by GRAPES-3 array during 1 January 2014 - 31 August 2016 is used for the analysis. The total live time of data collection is ≈ 926 days. The number of showers remaining after applying all the quality cuts are 3.2 $\times 10^7$ from a total set of 2.5 $\times$ 10^9 showers.

4. MC Simulations

A detailed simulation study is done to calculate the efficiency of the EAS detector array, its acceptance range and the energy calibration. Simulated EAS data for H, He, N, Al, and Fe is produced by using CORSIKA (version 7.69) simulation package. The N, Al and Fe are used to represent light (C, N, O), medium (Mg, Al, Si) and heavy (Mn, Fe, Co) masses in PCRs. For this analysis, data is generated with QGSJET-II-04 and FLUKA hadronic interaction models for high and low energy, respectively. Data is generated in the energy range of 1 TeV to 10 PeV and zenith angle range of 0° - 45°, following a power law with a spectral index of -2.5. For the analysis, each shower is thrown in a circular area of radius 150 m from the center (-13.85 m, 6.29 m) of the GRAPES-3 EAS detector array with a random core position. Each shower is reused 10 times to improve the statistics, which makes the total number of showers to be 1.2 $\times 10^9$. The GEANT-4 package is used to simulate the scintillator detector response. A detailed GEANT-4 simulation is carried out to study the response of the secondary particles in the muon telescope. Due to the sec(θ) GeV threshold of GRAPES-3 muon telescope for the secondaries incident at zenith angle θ, the soft component of the EAS gets filtered out. Therefore, for each triggered shower, the response of muon and hadron is measured in terms of PRC hits by using the GEANT-4 simulation. These PRC hits are used to count the muon tracks in the muon telescope.

5. Analysis

5.1 Efficiency and Acceptance

For each simulated element, the trigger efficiency (ϵ_T) and reconstruction efficiency (ϵ_R) are calculated as a function of primary energy. Total efficiency (ϵ_{tot}) is determined by the product

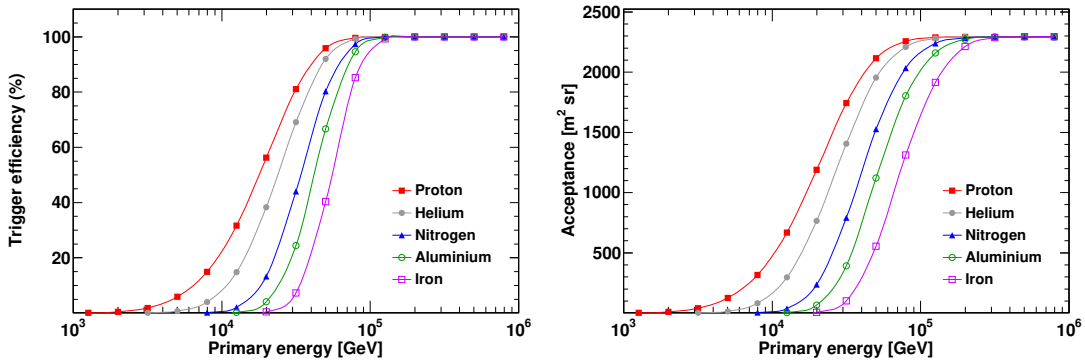

Figure 2: left: Trigger efficiency; right: acceptance as a function of primary energy for H, He, N, Al and Fe.

of trigger and reconstruction efficiencies. Acceptance (A_{acc}) is represented as the product of the effective area and the effective viewing angle as

$$A_{acc}(E_T) = \frac{\pi A}{2} \sum_{k=1}^{n_\theta} \varepsilon_{tot}(E_T, \theta_k)(cos2\theta_k - cos2\theta_{k+1}), \tag{2}$$

where A is the fiducial area, n_θ is the total number of angle bins and θ_k and θ_{k+1} are low and high edges of each angle bin, respectively. The trigger efficiency and acceptance of each simulated element are shown in Figure 2. The trigger efficiency is >90% at 50 TeV, 55 TeV, 60 TeV, 80 TeV and 100 TeV for H, He, N, Al and Fe, respectively. The acceptance is increased to 2300 $m^2 sr$ at 100% efficiency for $\theta < 18°$.

5.2 Elemental composition

The GRAPES-3 muon telescope is dedicated to measure the number of secondary muon tracks for each triggered shower. If the number of incident muons is small, the muon detection process is reliable. With the increase in the energy of PCRs, the number of muons increase which leads to the overlapping of muon tracks. Therefore, the number of detected muons is underestimated. This saturation effect is studied in each muon module (35 m^2) through simulations and the result of one module is displayed in Figure 3. For example, on average, ten incident muons get reconstructed as eight detected muons. To correct for the saturation, the saturation curve is modelled with a 3^{rd} order polynomial for detected muons ≥ 4. This correction is applied to each triggered shower to get the correct estimate of the muon multiplicity. The muon multiplicity distributions (MMDs) for all simulated primaries, for $4.4 \leq \log(N_e) < 4.6$, are shown in Figure 3. For a given shower size, the mean value of MMD increases with the mass number of the PCRs which indicates that the MMD is sensitive to the composition of the PCRs.

The shape of muon multiplicity distribution is well described by the negative binomial distribution (NBD) and is given by

$$NBD = \frac{\Gamma(x+r)}{\Gamma(x+1)\Gamma(r)} \left(\frac{r}{r+m}\right)^r \left(\frac{m}{r+m}\right)^x, \tag{3}$$

where m is the mean value of MMD and r is a measure of the standard deviation of the distribution. Therefore, the normalized MMD of each simulated primary is fitted with NBD to model statistical

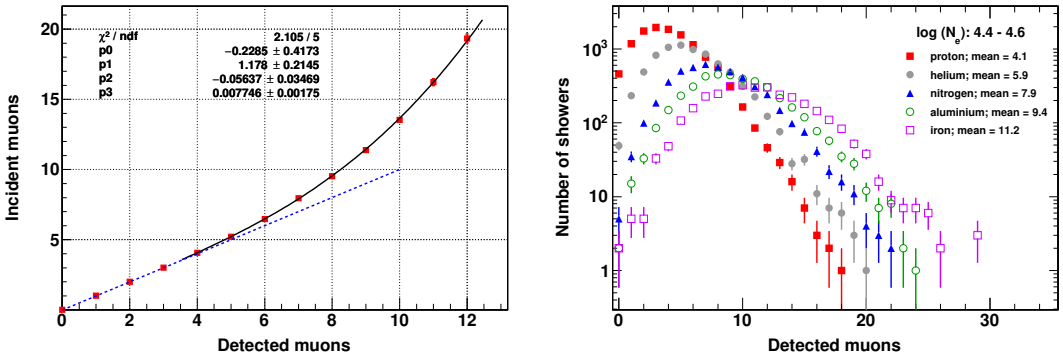

Figure 3: left: Muon saturation curve for one module of muon telescope, fitted with 3^{rd} order polynomial. right: Muon multiplicity distribution for all simulated primaries, for $4.4 \leq \log(N_e) < 4.6$.

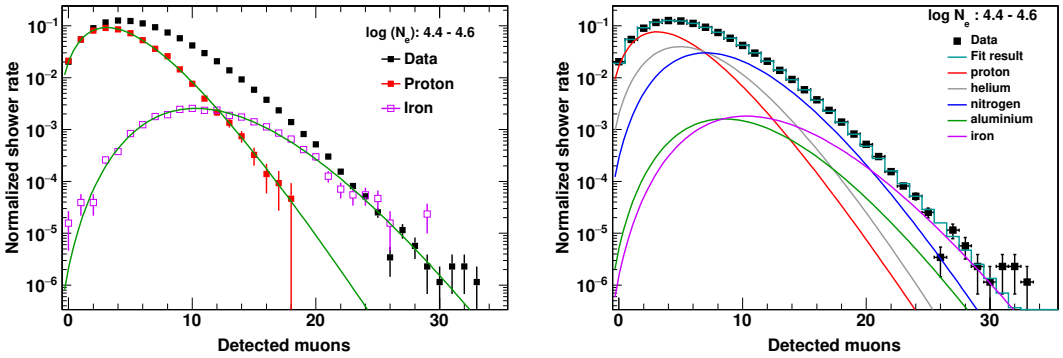

Figure 4: left: Muon multiplicity of H and Fe fitted with the negative binomial distribution, plotted along with experimental data. right: χ^2 minimization of normalized MMD for simulated primaries with observed normalized MMD; for $4.4 \leq \log(N_e) < 4.6$.

fluctuations. The fit results for proton and iron along with observed MMD, for $4.4 \leq \log(N_e) < 4.6$, are shown in Figure 4. The distribution of proton and iron are scaled such that the tails of distribution overlap with the observed MMD. The low multiplicity of observed MMD is well described by the proton while higher multiplicity is well described by the iron. However, to describe the middle range of the observed MMD, primaries of intermediate-mass number are required. The relative abundance of each simulated primary is extracted by minimizing the χ^2 of normalized MMD function of each simulated primary with normalized observed MMD,

$$\chi^2 = \sum_i \frac{(d_i - \sum_j a_j n_{ji})^2}{\epsilon_i^2} \tag{4}$$

where d_i and ϵ_i are respectively the value and uncertainty of the normalized observed MMD in the i^{th} bin, n_{ji} is the value of NBD function of j^{th} simulated primary in the i^{th} bin of data, a_j is the relative abundance of j^{th} primary.

The MMDs for Al and Fe overlap substantially. Hence, for this analysis, they are combined by assuming a ratio of Al/Fe = 0.8 based on the results of a direct detection experiment [5]. Since the abundance ratio Al/Fe is fixed, effectively the number of independent primaries is reduced to 4.

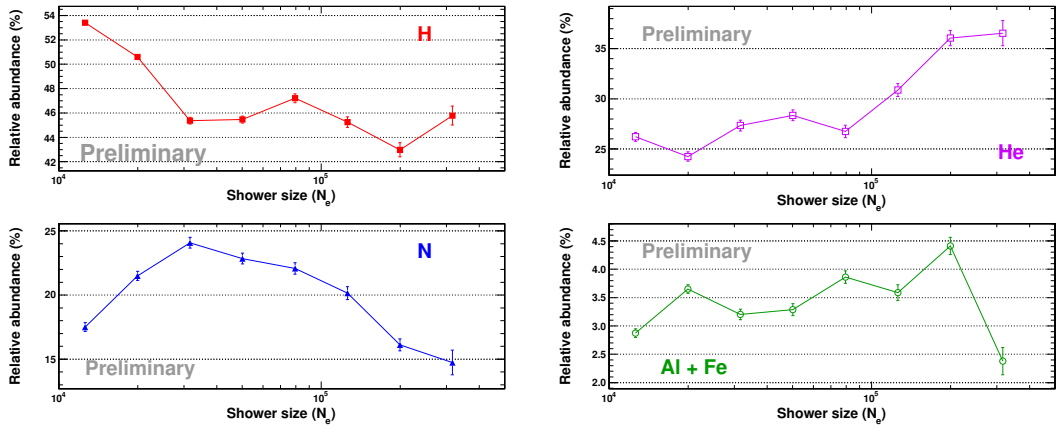

Figure 5: Relative abundance of all the simulated primaries; H, He, N and Al+Fe.

TMinuit is used for the minimization of χ^2. The fit results of χ^2 minimization for $4.4 \leq \log(N_e) < 4.6$ is shown in Figure 4.

6. Results

The measured relative abundances are shown in Figure 5. The relative abundance of proton decreases from 53% at shower size $10^{4.1}$ to 43% at shower size $10^{5.3}$. The relative abundance of helium increases from 26% at shower size $10^{4.1}$ to 36% at shower size $10^{5.3}$. The relative abundance of nitrogen first increases from 17% at shower size $10^{4.1}$ to 24% at shower size $10^{4.3}$ and then decreases to 16% at shower size $10^{5.3}$. The combined relative abundance of aluminium and iron increases from 2.9% at shower size $10^{4.1}$ to 4.4% at shower size $10^{5.3}$. The relative abundance is used to decouple the observed shower size distributions into elemental shower size distribution for the shower size range $10^{4.0}$ to $10^{5.6}$. A detailed study is conducted to get energy distribution from the shower size distribution. For this work, the energy distribution of simulated primaries is studied for a given shower size bin. In the interesting range of shower size (where efficiency is greater than 90%), the energy distribution, in a given shower size bin, can be approximate with a Gaussian on log scale. So, with the help of a Gaussian random number generator, the distribution of energy is generated for a given shower size. The differential cosmic-ray spectrum (dI/dE) can be expressed as follows,

$$\frac{dI}{dE} = \frac{1}{T_{obs}} \left(\frac{N}{\Delta E \cdot A_{acc}} \right)_i \tag{5}$$

where the subscript i denotes the i^{th} energy bin, N is the number of EAS, ΔE is the width of energy bin, A_{acc} is acceptance for the i^{th} energy bin and T_{obs} is the live time of the data. The measured preliminary elemental spectrum of proton and helium are plotted with direct and indirect observations [6, 14] in Figures 6 and 7, respectively. The statistical error bars are smaller than the marker size. The flux of the measured proton spectrum in this work is consistent with CREAM I+ III [9] and NUCLEON KLEM [8] (within error) at lower energy and is consistent with KASCADE (QGSJET-01) [14] at higher energy. Similarly, the measured Helium is consistent with CREAM I+ III and NUCLEON KLEM (within error) at lower energy.

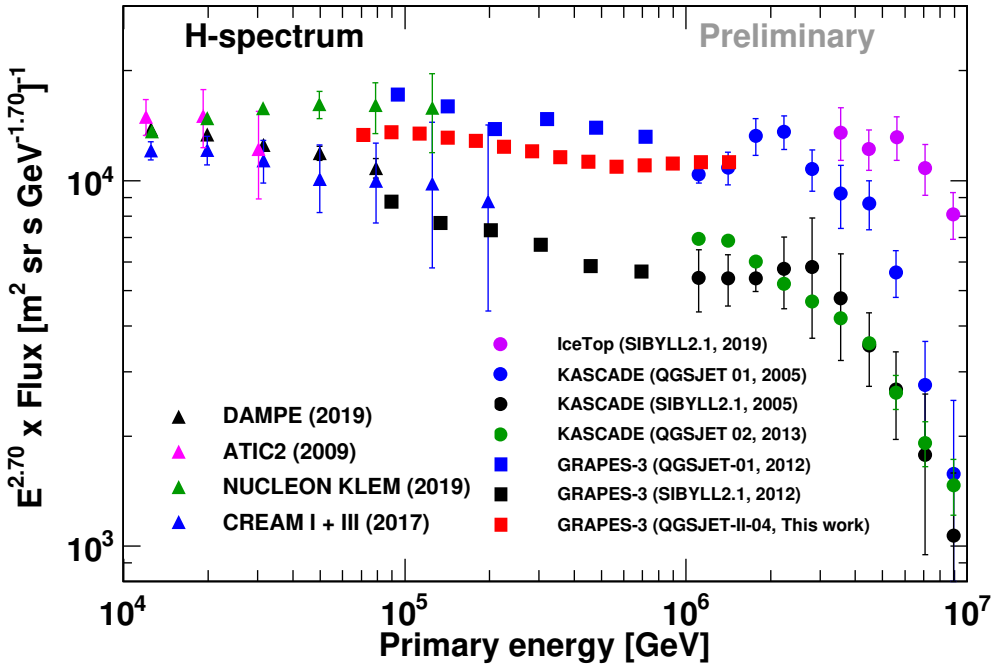

Figure 6: Elemental spectrum of proton; compared with other experiments.

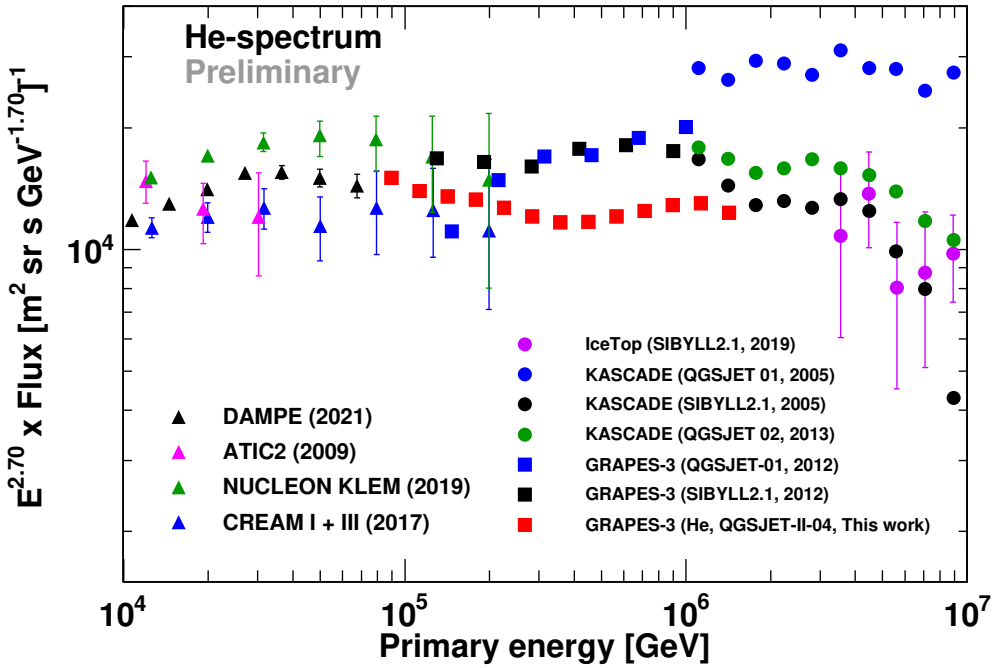

Figure 7: Elemental spectrum of helium; compared with other experiments.

7. Acknowledgements

We thank D.B. Arjunan, S. Kingston, K. Manjunath, S. Murugapandian, B. Rajesh, M.S. Shareef, C. Shobana, R. Sureshkumar and other colleagues for their help in running and maintenance of the GRAPES-3 experiment. We are also thankful to the staff of TIFR Computer Center and Communication Facility for providing access to the new HPC (High-Performance Computing) facility for the required simulations. A part of the Monte Carlo data production of this work is carried out on the PC cluster at Center for Computational Astrophysics, National Astronomical Observatory of Japan.

References

[1] S.K. Gupta et al., Nucl. Instrum. Methods A 540 (2005) 311.
[2] P.K. Mohanty et al., Astropart. Phys. 31 (2009) 24.
[3] Y. Hayashi et al., Nucl. Instrum. Methods A 545 (2005) 643.
[4] V.B. Jhansi et al., JCAP07 (2020) 24.
[5] Shibata T. et al., Astropart. Phys. 16 (2001) 13.
Derbina V. A et al., Astrophys. J. Lett. 628 (2005) L41.
[6] F. Alemanno et al., Phys. Rev. Lett. 126 (2021) 201102.
[7] Q. An et al., Sci. Adv. 5 (2019) eaax3793.
[8] E. V. Atkin et al., Astronomy Reports 63 (2019) 1.
[9] Yoon et al., The Astrophys. J. 839 (2017) 5.
[10] Panov et al., Bulletin of the Russian Academy of Sciences: Physics, 73 (2009) 564.
[11] M.G. Aartsen et al., Phys. Rev. D 100 (2019) 082002.
[12] W.D. Apel et al., Astropart. Phys. 47 (2013) 54.
[13] H. Tanaka et al., Nucl. Part. Phys. 39 (2012) 025201.
[14] T. Antoni et al., Astropart. Phys. 24 (2005) 1.